

## On the Application of Open-Path Fourier Transform Infra-Red Spectroscopy To Measure Aerosols: Observations of Water Droplets

RAM A. HASHMONAY\* AND  
MICHAEL G. YOST

Department of Environmental Health, Mail Box 357234,  
University of Washington, Seattle, Washington 98195

This paper proposes the application of Open-Path Fourier Transform Infra-Red (OP-FITR) spectroscopy to measure aerosols. A preliminary experiment conducted in a standard shower chamber generated a condensed water aerosol cloud. The OP-FITR beam acquired spectra through the cloud of water droplets. We matched calculated extinction spectra to measured extinction in the spectral range between 500 and 5000 wavenumbers by using Mie theory for spherical particles. The results indicate that size distribution parameters may be retrieved from OP-FITR spectra acquired over a 1 km optical path with reasonable detection limits on the order of  $10 \mu\text{g}\cdot\text{m}^{-3}$  for aerosols with optical properties equivalent to water.

### Introduction

Open-Path Fourier Transform Infra-Red (OP-FITR) spectroscopy is a well accepted technology designed for measuring gaseous air contaminants. OP-FITR absorbance spectra acquired during changing aerosol conditions reveal related changes in very broad features of the baseline. Usually this "shearing" of a spectrum's baseline is viewed as undesirable, because it interferes with quantifying gases. Arnot et al. applied FITR spectrometer measurements to study laboratory water clouds with a nearly constant size distribution (1). We demonstrate that these wavelength-dependent baseline features can be quantitatively related to changes in the aerosol size distribution. In this paper, we present preliminary results from OP-FITR measurements conducted in a standard shower chamber that generated a water condensation aerosol. We applied Mie theory (2) for spherical particles to an assumed size distribution function and known complex refractive index to match the measured extinction spectrum.

### Theoretical Extinction Spectrum

Light extinction due to aerosol as a function of wavelength can be computed by Mie theory if the complex refractive index as a function of wavelength and the aerosol size distribution are known. The extinction efficiency is a function of the particle size, light wavelength, and the complex refractive index  $m$  at the corresponding wavelengths. The relevant size parameter  $x$  of Mie theory (2) for monochromatic light is defined as the ratio between the particle diameter  $d$  and the wavelength  $\lambda$  multiplied by  $\pi$ . However, when a broad

spectral band of incident light is detected, one has to calculate the extinction efficiency for each combination of particle size and wavelength, due to changes in the complex refractive index over the spectral domain.

The extinction efficiency  $Q_e$  for a given  $m$  and  $x$  is a function of the Mie coefficients,  $a_n$  and  $b_n$ , (2). Our method for calculating the Mie coefficients followed the recurrence procedure in Wickramasinghe (3). We used the complex refractive index for water as measured by Wieliczka et al. (as shown in Figure 1a) (4). We summarized the extinction efficiency values in a matrix  $Q_{ej}$  where each row ( $i$ ) is for a different wavelength (or wavenumber) and each column ( $j$ ) is for a different particle size class. We expressed the spectral domain in wavenumbers ( $\text{cm}^{-1}$ ) for comparison with the OP-FITR spectrum. We calculated the extinction efficiency matrix  $Q_{ej}$  for 1125 wavenumber values over the range of  $500-5000 \text{ cm}^{-1}$  ( $20-2 \mu\text{m}$  respectively) and for 32 diameter size values between 1 and  $32 \mu\text{m}$ . Following Hinds (5), we expressed the extinction coefficient  $\sigma_e$  in  $\text{cm}^{-1}$  as a function of wavelength and for a given size distribution as

$$\sigma_e = \frac{\pi}{4} \sum_j Q_{ej} N_j d_j^2 \quad (1)$$

where  $N_j$  is the number density at the  $j$ th particle size class in  $\text{cm}^{-3}$ ;  $d_j$  is the mean diameter of the  $j$ th particle size class in cm;  $i$  is the index number for the wavelength; and  $j$  is the index number for the particle size class. Multiplying the extinction coefficient by the OP-FITR beam path length gives the unitless extinction spectrum which is the same as the absorbance spectrum.

### Experimental Setup

A series of controlled experiments with condensed water aerosol were conducted to test the feasibility of measuring aerosol size distributions with OP-FITR. A Nicolet OP-FITR was used for the experiment (6). The modulated beam passed through a cloud of water droplets to a telescope focused onto a liquid nitrogen cooled Mercury Cadmium Telluride detector at the opposite end of the standard shower chamber. The dimensions of the standard shower chamber were 0.85 m width, 1.18 m length, and 1.53 m height. The chamber was constructed using 1.75 cm thick plexiglass. An exhaust hole, 9 cm in diameter, on the chamber ceiling was used to ventilate the system. The hole was fitted with a plastic T-joint to allow both the water pipe and exhaust air from a small fan to pass through the same opening. The air flow rate measured from the exhaust fan was  $0.5 \pm 0.1 \text{ m}^3/\text{s}$ . Two 6.4 cm diameter air inlets were located on opposite walls, 110 cm above the chamber floor. These holes allowed the bistatic OP-FITR modulated beam to pass through the chamber walls into the detector located 1 m away. These holes were positioned so the beam did not pass directly through the shower water spray.

We analyzed data from two shower experiments at two different inlet water temperature conditions 40 and  $52 \text{ }^\circ\text{C}$ . In each experiment, the water was turned on for a 10 min period, and OP-FITR measurements started when the water was turned on and continued for 15 min. The OP-FITR interferometer sampled at a rate of 1.7 spectra/min, and each spectrum included 48 coadded scans at a resolution of  $2 \text{ cm}^{-1}$ . Prior to each experiment a background interferogram was collected with 1280 coadded scans (approximately 10

\* Corresponding author phone: (206)685-4471; fax: (206)616-2687; e-mail: ramha@u.washington.edu.

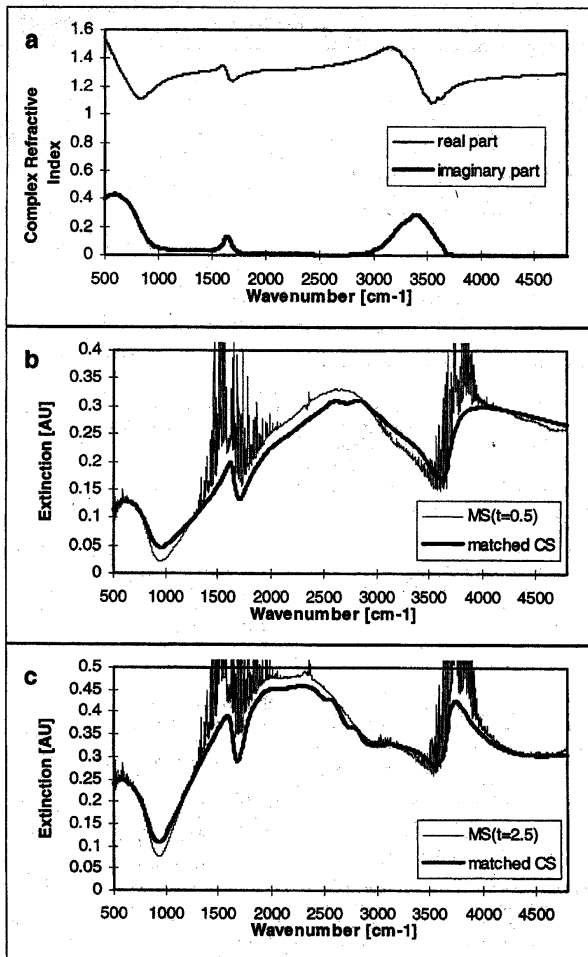


**FIGURE 1.** Summary of experimental results and computations based on Mie theory for spherical particles and the complex refractive index of water: (a) complex refractive index function for liquid water as measured by Wieliczka et al. (4); (b) measured spectrum (MS) at  $t = 0.5$  min and calculated spectrum (CS) assuming a Gaussian size distribution with average concentration of  $0.4 \text{ g}\cdot\text{m}^{-3}$ , mean diameter =  $7 \mu\text{m}$ , and  $\text{SD} = 2 \mu\text{m}$ ; (c) MS at  $t = 2.5$  min and CS assuming an average concentration of  $0.5 \text{ g}\cdot\text{m}^{-3}$ , mean diameter =  $10 \mu\text{m}$ , and  $\text{SD} = 2 \mu\text{m}$ .

min). More details of the shower setup and experiment procedures are described in the work of Keating et al. (7).

### Results and Discussion

Each measurement over time produced different absorbance baseline features in the spectral domain. Since condensed water droplets are approximately spherical and have a known complex index of refraction, we could compute the extinction spectra for assumed size distributions.

We used the above procedure to calculate the extinction spectrum for different assumed mass size distribution

functions. We used complex refractive index values measured at room temperature (4). The air temperatures measured inside the shower chamber ranged from 15 to 25 °C during the experiments. Temperature changes in this range have almost no impact on the complex refractive index values over the measurement spectral range (8). Consequently, temperature has no impact on the calculated extinction spectrum. For calculation purposes, we converted the mass size distributions to the number density size distributions ( $N$  in eq 1). We manually changed the distribution parameters to iteratively match a calculated extinction spectrum to the

measured OP-FTR spectrum baseline. We found that calculated spectra matched well with the measured spectra baselines when we assumed Gaussian mass size distributions with standard deviations around  $2 \mu\text{m}$  and means in the range of  $6-11 \mu\text{m}$ . Each matched spectrum corresponded to a unique set of Gaussian parameters. All the computed and measured spectra had three distinct minima at the same locations at about  $950, 1650,$  and  $3500 \text{ cm}^{-1}$  which correspond primarily to minima in the real part of the complex refractive index as shown in Figure 1a.

In Figure 1b,c we present examples of two measured spectra (MS) from the OP-FTR experiment at  $52^\circ\text{C}$  inlet water temperature along with the matched computed spectra (CS). The comparisons represent examples from the OP-FTR measurements acquired at  $0.5 \text{ min}$  ( $\text{MS}(\tau = 0.5)$ ) and at  $2.5 \text{ min}$  ( $\text{MS}(\tau = 2.5)$ ) after the water started. During this time period we observed the largest transition in the measured extinction spectra, reflecting changes in aerosol size distribution. In the period between 3 and 10 min the shape of the spectral baseline changed very little but decreased somewhat in scale. After 10 min the water was turned off and the cloud rapidly disappeared. In the experiment illustrated here a consistent trend in the physical process was observed both in the measured spectrum (OP-FTR) and the matched calculated spectrum. Shortly after the water in the shower was turned on, the aerosol consisted mostly of fine condensation droplets, and during the first 2 min the aerosol average diameter increased toward coarser droplets. At approximately 3 min into the experiment the aerosol size proportions reached steady-state conditions, presumably an equilibrium of condensation vs evaporation. This phenomenon was repeated in the shower experiment conducted with water temperatures of  $40^\circ\text{C}$ .

The location of the three minima of the spectra baseline are due to the complex refractive index function and are independent of the size distribution. These minima behave like a signature of water aerosol in this spectral range. The MS also show many sharp water vapor absorption lines at about  $1500$  and  $3500 \text{ cm}^{-1}$ , roughly corresponding to peaks in the imaginary part of the complex refractive index of liquid water.

Figure 1b overlays a matched calculated spectrum onto the measured spectrum at  $t = 0.5 \text{ min}$ . The matched spectrum in Figure 1b corresponds to a Gaussian particle mass distribution with these parameters: mean diameter of  $7 \mu\text{m}$ , standard deviation of  $2 \mu\text{m}$ , and average concentration of  $0.4 \text{ g}\cdot\text{m}^{-3}$ . Figure 1c presents the second example calculated as above but for the measured spectrum at  $t = 2.5 \text{ min}$ . The matched spectrum in Figure 1c corresponds to a Gaussian distribution with a mean diameter of  $10 \mu\text{m}$ , standard deviation of  $2 \mu\text{m}$ , and average concentration of  $0.9 \text{ g}\cdot\text{m}^{-3}$ . These size values correspond to the smaller portion of the size range in atmospheric fog and mist ( $2-200 \text{ microns}$ ) (5).

The measured spectra in Figure 1b,c show some notable trends over time. The peak in the extinction in Figure 1b at  $t = 0.5 \text{ min}$  appears around  $2700 \text{ cm}^{-1}$  ( $\sim 3.7 \mu\text{m}$ ). Two min later, the peak in extinction is shifted toward smaller wavenumbers (i.e. longer wavelengths) around  $2200 \text{ cm}^{-1}$  ( $\sim 4.5 \mu\text{m}$ ) suggesting the presence of larger particles (Figure 1c). In the later sample, the overall extinction also increased indicating an increase in the total cross section area or more particles. A similar pattern was found in the size distributions needed to match the calculated spectra, which suggests a shift toward larger particles and a higher average mass concentration in the later sample. Overall, the extinction spectra in Figure 1b,c indicate that as the particle size increased, the peaks in the baseline extinction features of the measured spectra shifted toward smaller wavenumbers (longer wavelengths).

The calculated extinction functions and measured baselines for infrared spectra in the presence of water aerosol matched quite well. Some mismatch or error is present in the calculated spectra, but overall there is substantial agreement with the baseline features of the measured spectra. The errors are probably due to our manual matching of the aerosol size distribution parameters and our choice of a Gaussian distribution shape. Our manual matching procedure using successive approximation was not optimized in terms of "least squares" or any other objective criteria. A more sophisticated numerical fitting procedure probably could be developed to address these limitations and obtain a more detailed estimate of the aerosol size distribution parameters.

Our observations indicate that the complex refractive index function of the aerosol is the key information needed to account for the broad absorbance features in the baseline of an OP-FTR spectrum measured in the presence of aerosols. With some knowledge of the complex refractive index function for the specific aerosol material and the measured infrared spectrum, it should be possible to estimate the aerosol size distribution parameters in near real time. In many cases of outdoor long-path monitoring, we have observed very broad absorption features that may be related to particle extinction. However, we found it impossible to analyze these features for the aerosol size distribution because we lacked knowledge on the optical properties of the relevant aerosols. Further research on the infrared optical properties of common urban aerosols must be conducted to push forward this idea. Realizing this goal also requires the development of inversion methods to recover the size distribution of the aerosol from the absorbance features in the OP-FTR spectrum baseline. This raises the interesting possibility of using OP-FTR to simultaneously measure both pollutant gases and aerosols (7).

Like gas measurements, detection limits for aerosol measurements strongly depend on the optical properties of the material, the background spectrum, and on the path length. A "cleaner" background spectrum and longer path length will lower the detection limit for a given material. Our measurements represent a dense water aerosol ( $> 0.4 \text{ g}\cdot\text{m}^{-3}$ ) over a 1 m beam path which produced absorbance values higher than  $0.1$  absorbance units (AU). These readings suggest that for aerosols with equivalent extinction to water droplets of  $7 \mu\text{m}$  mean diameter, average concentrations of approximately  $10 \mu\text{g}\cdot\text{m}^{-3}$  should be detectable over a 1 km optical path. This is based on a conservative rms noise level of  $10^{-3}$  AU for a low spectral resolution open path spectrometer and a minimum signal-to-noise ratio of 3.

The preliminary results of this study provide a physical explanation for the observed baseline absorbance features in an OP-FTR spectrum in the presence of aerosols. Application of this work could broaden the scope of OP-FTR applications to include real time determination of path-averaged aerosol concentrations and size distribution parameters.

## Acknowledgments

This research was partially supported by the Consortium for Risk Evaluation with Stakeholder Participation (CRESP) through U.S. Department of Energy (DOE) Cooperative Agreement No. DE-FC01-95EW55084 and by the National Institute for Occupational Safety and Health (NIOSH) through Grant R01OH02560. This support does not constitute an endorsement by DOE or NIOSH of the views expressed in this article. We also thank Robert S. Crampton, a graduate research assistant, for preparing the measured absorbance spectra.

## Literature Cited

- (1) Arnot, W. P.; Schmitt, C.; Yangang, L.; Hallett, J. *Appl. Opt.* 1997, 36, 5205.
- (2) Bohren, C. F.; Huffman, D. R. *Absorption and Scattering of Light by Small Particles*; John Wiley & Sons: New York, 1983.
- (3) Wickramasinghe, N. C. *Light Scattering Functions for Small Particles with Applications in Astronomy*; Adam Hilger: London, 1973; pp 25-27.
- (4) Wleliczka, D. M.; Weng, S.; Querry, M. R. *Appl. Opt.* 1989, 28, 1714.
- (5) Hinds, W. C. *Aerosol Technology*; John Wiley & Sons: New York, 1982; p 320.
- (6) Xiao, H. K.; Levine, S. P.; Herget, W. F.; D'Arcy, J. B.; Spear, R. C.; Pritchett, T. A. *Am. Ind. Hyg. Assoc. J.* 1991, 52, 449.
- (7) Keating, G. A.; McKone, T. E.; Gillett, J. W. *Atmospheric Environ.* 1997, 31(2), 123.
- (8) Ray, P. S. *Appl. Opt.* 1972, 11, 1836-1844.

*Received for review August 10, 1998. Revised manuscript received December 21, 1998. Accepted January 25, 1999.*

ES980813B

## More than low flow

According to recent work by Thomas Dülcks and co-workers at the University of Frankfurt (Germany), nanoelectrospray is more than just a scaled-down version of conventional electrospray (ionspray).

Electrospray can be roughly divided into two steps. First, the sample liquid is dispersed into charged droplets. Second, the initial droplets decompose via solvent evaporation into smaller and more highly charged droplets. After successive fissions, a droplet is small enough to release ions. The second part of the process has been extensively studied. Droplet formation has received much less attention.

To determine how initial droplet size affects the mass spectrum, Dülcks and his co-workers analyzed a salt solution (NaCl), a peptide/salt solution (bovine insulin and NaCl), and a sugar/salt solution (maltopentaose and NaCl) by nanoelectrospray MS and ionspray MS. In all three cases, the ionspray mass spectrum was much "noisier" even though the initial concentrations of the solutions were identical.

The authors suggest that the chemical noise is caused by ionspray droplets becoming more concentrated as they go through additional fission steps. Ionspray, therefore, encourages the formation of salt cluster ions. Because nanoelectrospray droplets are much smaller to begin with, only one fission is usually required before an ion is released. Therefore, the concentration in the droplet does not increase significantly. In general, nanoelectrospray can tolerate salt concentrations an order of magnitude higher than ionspray.

Nanoelectrospray was the only method that yielded a useful mass spectrum for the sugar and salt mixture. Oligosaccharides are difficult to analyze by ionspray because they are not enriched at the droplet surface, so sugar and salt clusters are released by the same fission pathway. According to the authors, this improvement relative to ionspray is due to "noise" originating from highly concentrated residue droplets occurs to a lesser extent than in ionspray.

Interestingly, the authors observed salt cluster ions of the form  $(\text{NaCl})_n\text{Na}^+$ , with

$n > 30$ . Such large cluster ions had not previously been observed, and their absence had been seen as evidence of electrospray ion formation according to field evaporation processes. According to the authors, these clusters present evidence that they were formed by evaporation of nanodroplets containing high salt concentrations rather than by field evaporation processes. (*J. Am. Soc. Mass Spectrom.* 1999, 10, 300-08)

## Beaming through water droplets

Open-path (OP) FT-IR, a technique designed for measuring gaseous air pollutants, works poorly in the presence of aerosols. Changing aerosol conditions affect the baseline and shift peaks, making it difficult to quantify gases. Ram A. Hashmonay and Michael G. Yost of the University of Washington provide clues as to why these spectral changes occur.

In a series of experiments conducted in a shower chamber, the researchers gener-

## Molecular beacons put down roots

Molecular beacons (MBs) are single-stranded oligonucleotide probes that are used to detect complementary DNA sequences. Weihong Tan and colleagues at the University of Florida have found a way to anchor MBs, which are normally used in solution, to silica surfaces using biotin and avidin.

An MB begins as a stem-and-loop structure with a fluorophore at one end and a quencher at the other. The stem is formed from the five bases at the fluorophore's end and the five bases at the quencher's end. These sets of bases are complementary, allowing the ends to hybridize. The rest of the probe—the loop—remains unhybridized and serves as the probe's active area. The loop varies in length and sequence depending on the application.

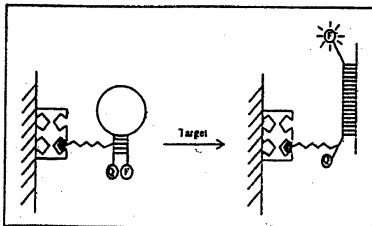
When the MB is in this stem-and-loop structure, the fluorophore and quencher are next to each other, and there is

little fluorescence. The situation is different when a complementary DNA sequence is present. Because all of the complement's bases match the MB, hybridization between these two sequences is much stronger than self-hybridization in the stem. Thus, the MB preferentially hybridizes to its complement, unfolding in the process and separating the fluorophore from the quencher. The fluorescence signal becomes more intense, essentially serving as

a beacon to indicate the presence of the complementary sequence.

To keep the hybridization process intact while attaching the MB to a silica surface, Tan and colleagues added a biotin label to the stem of folded MB, and they treated the silica surface with avidin, using glutaraldehyde as a cross-linking agent. Then the researchers allowed the biotinylated MB to bind to the avidin-conjugated surface, creating a plate covered with DNA probes.

The performance of the MB-immobilized plate was tested using different concentrations (5–600 nM) of the complementary sequence. The researchers reported that they could detect subnanomolar amounts of the target DNA and that the plate could be reused multiple times. The researchers also noted that the high specificity and sensitivity of the MBs should make these plates useful in DNA sensors for monitoring single cells or studying DNA molecular dynamic interactions. (*J. Am. Chem. Soc.* 1999, 121, 2921–22)



A folded, biotinylated molecular beacon is bound to an avidin-conjugated surface. Because the fluorophore and quencher are close together, there is little fluorescence. After the target DNA is added, the molecular beacon hybridizes to it, unfolding in the process. This separates the fluorophore and the quencher, generating an intense fluorescence signal.